10-2011

Quantified H i morphology – I. Multi-wavelength analysis of the THINGS galaxies.

Benne W. Holwerda
University of Louisville

N. Pirzkal
Space Telescope Science Institute

W. J. G. de Blok
University of Cape Town

A. Bouchard
McGill University

S. -L. Blyth
University of Cape Town

See next page for additional authors

Original Publication Information

Holwerda, B. W., et al. "Quantified H I Morphology – I. Multi-wavelength Analysis of the THINGS Galaxies." 2011. *Monthly Notices of the Royal Astronomical Society* 416(4): 2401-2414.

Monthly Notices
of the
ROYAL ASTRONOMICAL SOCIETY

Mon. Not. R. Astron. Soc. **416,** 2401–2414 (2011) doi:10.1111/j.1365-2966.2011.18938.x

Quantified H I morphology – I. Multi-wavelength analysis of the THINGS galaxies

B. W. Holwerda,[1,2⋆] N. Pirzkal,[3] W. J. G. de Blok,[2] A. Bouchard,[4] S.-L. Blyth,[2] K. J. van der Heyden[2] and E. C. Elson[2]

[1] *European Space Agency, ESTEC, Keplerlaan 1, 2200 AG, Noordwijk, the Netherlands*
[2] *Astrophysics, Cosmology and Gravity Centre (ACGC), Astronomy Department, University of Cape Town, Private Bag X3, 7700 Rondebosch, Republic of South Africa*
[3] *Space Telescope Science Institute, 3700 San Martin Drive, Baltimore, MD 21218, USA*
[4] *Department of Physics, Rutherford Physics Building, McGill University, 3600 University Street, Montreal, Quebec, H3A 2T8, Canada*

Accepted 2011 April 19. Received 2011 April 12; in original form 2010 January 22

ABSTRACT

Galaxy evolution is driven to a large extent by interactions and mergers with other galaxies and the gas in galaxies is extremely sensitive to the interactions. One method to measure such interactions uses the quantified morphology of galaxy images. Well-established parameters are Concentration, Asymmetry, Smoothness, Gini and M_{20} of a galaxy image. Thus far, the application of this technique has mostly been restricted to rest-frame ultraviolet and optical images. However, with the new radio observatories being commissioned [South African Karoo Array Telescope (MeerKAT), Australian SKA Pathfinder (ASKAP), Extended Very Large Array (EVLA), Westerbork Synthesis Radio Telescope/APERture Tile In Focus instrument (WSRT/APERTIF) and ultimately the Square Kilometer Array (SKA)], a new window on the neutral atomic hydrogen gas (H I) morphology of large numbers of galaxies will open up. The quantified morphology of gas discs of spirals can be an alternative indicator of the level and frequency of interaction. The H I in galaxies is typically spatially more extended and more sensitive to low-mass or weak interactions.

In this paper, we explore six morphological parameters calculated over the extent of the stellar (optical) disc and the extent of the gas disc for a range of wavelengths spanning ultraviolet (UV), optical, near- and far-infrared and 21 cm (H I) of 28 galaxies from The H I Nearby Galaxy Survey (THINGS). Although the THINGS sample is small and contains only a single ongoing interaction, it spans both non-interacting and post-interacting galaxies with a wealth of multi-wavelength data. We find that the choice of area for the computation of the morphological parameters is less of an issue than the wavelength at which they are measured. The signal of interaction is as good in the H I as at any of the other wavelengths at which morphology has been used to trace the interaction rate to date, mostly star formation dominated ones (near- and far-ultraviolet). The Asymmetry and M_{20} parameters are the ones that show the most promise as tracers of interaction in 21 cm line observations.

Key words: galaxies: fundamental parameters – galaxies: interactions – galaxies: kinematics and dynamics – galaxies: spiral – galaxies: structure.

1 INTRODUCTION

Evolution of galaxies in the cold dark matter with a cosmological constant (ΛCDM) universe appears to be driven by the merger and interaction of dark matter haloes (e.g. the Millennium Simulation by Springel et al. 2005). Therefore, a substantial observational effort has been made to quantify the rate of mergers and interactions over time. Several methods have been developed to estimate the interaction rate: identification of physically close pairs of galaxies in redshift surveys (e.g. Patton et al. 2000; de Ravel et al. 2009), measures of Hα equivalent width, far-IR flux from (ultra) luminous infrared galaxies [(U)LIRGs; see e.g. Murphy et al. 2001], from the starburst, OH megamasers (e.g. Klöckner & Baan 2005; Darling & Giovanelli 2006) and identification of galaxies with disturbed morphologies (e.g. Conselice 2003; Lotz, Primack

⋆E-mail: benne.holwerda@esa.int

& Madau 2004; Lotz et al. 2008a; Conselice, Yang & Bluck 2009). This observational effort has been matched by theoretical ones to accurately map the well-understood merger trees of dark matter haloes on to galaxy–galaxy merger rates (see the review in Hopkins et al. 2010, and references therein). Thus far, theoretical models suffer from large systematics. However, ongoing efforts in both cosmological hydrodynamical simulations and semi-analytical models can be expected to match the observational accuracy soon.

Merger rates from disturbed morphologies of galaxies have been explored extensively with quantified classification of galaxies. Based on a series of scale-invariant parameters, quantified galaxy morphology has been applied predominantly on rest-frame ultraviolet images of galaxies (e.g. Taylor-Mager et al. 2007). The advantages for optical or ultraviolet are that interacting galaxies are star forming and hence bright in the ultraviolet and blue side of the optical. Their morphology shows enhanced surface brightness and clear signs of disturbance. The high surface brightness ensures more complete samples for a given observation. Observationally, this approach is also attractive as it has the advantage of similar spatial resolution at high and low redshift, using the *Hubble Space Telescope* (*HST*) and *Galaxy Evolution Explorer* (*GALEX*) or Sloan Digital Sky Survey (SDSS), respectively. Disadvantages of this method are the time-lag for the interaction to trigger star formation, and modification of the morphology due to dust obscuration.

However, new windows for quantified morphology are opening up; the far-infrared emission from star formation and molecular gas is now resolved with *Herschel* and in the near future with the Atacama Large Millimeter/submillimeter Array (ALMA). The atomic gas with its many signatures of interaction (tails, bridges, beards, warps, clouds, etc.) will also be much better resolved with the commissioning of the Square Kilometer Array (SKA; Carilli & Rawlings 2004), and its precursors, the South African Karoo Array Telescope (MeerKAT; Jonas 2007; Booth et al. 2009; de Blok et al. 2009), the Australian SKA Pathfinder (ASKAP; Johnston et al. 2008), and the pathfinders, the Extended Very Large Array (EVLA; Napier 2006), and the APERture Tile In Focus instrument (APERTIF; Verheijen et al. 2008) on the Westerbork Synthesis Radio Telescope (WSRT). Spatial resolutions of these observations will start to rival those in the ultraviolet. H I morphology also appears to be very sensitive to the smaller interactions with tidal features often reported to be much more visible than at any other wavelength (see the 'H I Rogues Gallery'[1] compilation in Hibbard et al. 2001). Hence the morphology of galaxies at other wavelengths, especially H I, might be an equally good or surpassing indicator of tidal interaction than that of the ultraviolet and other star formation dominated emission. Notably, the envisaged all-sky surveys with ASKAP (WALLABY[2]), and the WSRT/APERTIF, will then provide an accurate census of mergers in the local Universe.

The aims for this paper are to explore (1) which wavelength shows the strongest signal of interaction, (2) which morphological parameters are the optimal discriminators for interaction and (3) over which area morphological parameters need to be computed. In a previous paper (Holwerda et al. 2009), we briefly highlight how well H I morphology shows the signal of interaction compared to the ultraviolet (UV), optical and far-infrared (FIR). In further papers, we define the H I parameter space to identify interacting galaxies (Holwerda et al. 2011a) using a sub-sample of WHISP,[3] we derive a time-scale for interactions to reside in this parameter space (Holwerda et al. 2011b), and infer the first interaction fraction and rate based on the WHISP survey (Holwerda et al. 2011c). The H I morphological phenomena in the Virgo cluster environment (e.g. ram-pressure stripping) are explored in Holwerda et al. (2011d).

In Section 2 we discuss our sample and data used; in Section 3 we discuss the morphological parameters, as well as effects of uncertainty and possible biases. Our results are given in Section 4, together with notes on each individual galaxy. Our discussion on the suitability of the H I parameters is given in Section 6 and our conclusions are summarized in Section 7.

2 SAMPLE AND DATA

We use the public data sets from The H I Nearby Galaxy Survey (THINGS; Walter et al. 2008),[4] the *Spitzer* Infrared Nearby Galaxies Survey (SINGS; Kennicutt et al. 2003),[5] the *GALEX* Nearby Galaxy Atlas (NGA)[6] and the SDSS Data Release 7 (DR7).[7] Table A2 (in the electronic version of the article – see Supporting Information) lists the availability of *Spitzer*, *GALEX* and SDSS data for our sample, as well as the basic data from Walter et al. (2008). Optical data are from the SINGS ancillary data, the NASA Extragalactic Data base[8] public data or SDSS, preferring SDSS. We aim to cover the sample from Trachternach et al. (2008) and de Blok et al. (2008) because for these galaxies there is detailed dynamical information (rotation curves, dynamical centre and parametrizations of non-circular motions). We require H I data from the THINGS sample, *Spitzer* data from the SINGS sample of a programme with equivalent quality data and at least some optical data. These requirements narrow the 34 galaxies from Walter et al. (2008) down to 28.

The H I column density maps are the naturally weighted (NA) and robust-weighted (RO) total intensity maps, expressed as H I column density using the formalism and beam sizes reported in Walter et al. (2008). We chose the naturally weighted maps to define our contours as these are more sensitive to larger scale structures (of the order of the disc) than the robust weighted maps. The naturally weighted maps have lower spatial resolution (typically of the order of 10 arcsec resolution) than the robust-weighted ones (typically 6 arcsec). We compute morphological parameters for both H I maps. To define the area over which parameters are computed, we picked two H I column density contours: 0.3 and 30×10^{20} cm^{-2}. These correspond to approximately the spatial extent of the H I and stellar disc, respectively, but may exclude areas corresponding to 'H I holes'.

The majority of the *Spitzer* IRAC and MIPS data are from the SINGS project with three additions from the Local Volume Legacy Survey (LVL; Lee et al. 2008): NGC 5236 (M83), NGC 5457 (M101) and IC 2574. *Spitzer* data include all IRAC (3.6, 4.5, 5.6 and 8.0 μm) and MIPS (24, 70 and 160 μm) channels. These tend to comfortably cover the stellar disc and most of the H I outer contour (3×10^{19} cm^{-2}).

In the case of the SDSS optical data, we obtained the original tiles around our galaxies and combined them into larger mosaics using

[1] http://www.nrao.edu/astrores/HIrogues/

[2] Widefield ASKAP L-band Legacy All-sky Blind surveY.

[3] The Westerbork observations of neutral Hydrogen in Irregular and SPiral galaxies project (van der Hulst et al. 2001; van der Hulst 2002).

[4] http://www.mpia-hd.mpg.de/THINGS/

[5] http://sings.stsci.edu/

[6] http://galex.stsci.edu/GR4/

[7] http://cas.sdss.org/dr7/

[8] NED, http://nedwww.ipac.caltech.edu/

SWARP (http://astromatic.iap.fr/). The images were sky-subtracted before combination to account for the different sky values in each scan-strip. The SDSS mosaics have distinct advantages over the NED and SINGS ancillary data: uniform depth, a well-defined set of filters and a field-of-view that covers the whole H I map.

Most of the *GALEX* data are from the NGA supplemented with the all-sky survey in two cases: NGC 3184 and NGC 6946. NGA data generally mean the galaxy is in the focus of *GALEX* with 4 arcsec resolution in the far-UV (FUV) (1528 Å) and near-UV (NUV) (2271 Å). However, galaxies such as NGC 3031 and M81 Dwarf A are part of the M81/M82 group portrait and M83 is in the corner of the *GALEX* field of view because of a bright foreground star, and these galaxies are therefore slightly out-of-focus with *GALEX* with resolutions closer to 6 arcsec.

Table A1 (in the electronic version of the article – see Supporting Information) lists the resolutions and wavelength of all our data. *GALEX* resolution ranges from 4 to 6 arcsec depending on position in the field, MIPS at 24 μm is 6 arcsec and the RO maps are typically also 6 arcsec resolution, depending on the position in the sky and axis. The MIPS 70 and 160 μm and the NA maps are of poorer resolution.

2.1 Data preparation

To start, we shift the naturally weighted H I map, such that the centre of the galaxy is in the centre of the image. Because the THINGS observations are pointed, the galaxy is already close to the central part of the image and the shifts are small (a few pixels). We use the central positions reported in Walter et al. (2008), who list the dynamical central positions from Trachternach et al. (2008), supplemented on occasion with *Spitzer* 3.6 μm central positions. Subsequently, we align all the different data using WCSMAP and GEOTRAN in IRAF to this centred naturally weighted (NA) H I map. Our next step is to convolve the optical and IRAC data to 6 arcsec, approximately the resolution of the majority of the rest of the data, before determining the morphological parameters.

After alignment and smoothing, a mask of the foreground stars is created using a SExtractor (Bertin & Arnouts 1996; Holwerda 2005) catalogue and resulting segmentation map of the SDSS-i image, selecting small objects in the field. If the SDSS-i image is not available, we use the IRAC channel 2 (4.5 μm). Channels 1 and 2 of the IRAC instrument trace the old red stellar component, and we chose channel 2 as it does not contain the 3.1 μm polycyclic aromatic hydrocarbon (PAH) feature, so any hot interstellar medium (ISM) region that belongs to the galaxy is spuriously rejected. The disadvantage of the IRAC data is that it may not cover the entire gas disc but to mask foreground stars, it is preferable to use optical or near-infrared rather than *GALEX* data.

3 MORPHOLOGICAL PARAMETERS

The morphological parameters we use here have been established with repeated applications to deep *HST* images and reference local galaxy samples. There is the Concentration–Asymmetry–Smoothness (CAS) classification scheme and the Gini and M_{20} parameters. Ellipticity is sometimes added. We use the definitions shared by Conselice (2003), Lotz et al. (2004) and Scarlata et al. (2007) for our computation of the six morphological parameters: Concentration, Asymmetry, Smoothness, Gini, the moment of light (M_{20}) and Ellipticity.

3.1 CAS

Abraham et al. (1994, 1996a,b) introduced definitions of Asymmetry, Concentration and Contrast to classify galaxies in the *Hubble Deep Field*-North. Following the work by Bershady, Jangren & Conselice (2000) and Trujillo, Graham & Caon (2001c), Trujillo et al. (2001b) and Conselice, Bershady & Jangren (2000) refined these parameters, culminating in Conselice (2003) which added a local volume reference in *R* band (the sample from Frei et al. 1996). The thus-established parameter space has been used extensively on all *HST* wide and deep surveys: e.g. in GOODS by Bundy, Ellis & Conselice (2005) and Ravindranath et al. (2006), the HUDF by Yan et al. (2005), COSMOS by Scarlata et al. (2007), GEMS by Jogee et al. (2009) and the extended Groth strip by Trujillo et al. (2007).

3.1.1 Concentration

Concentration is defined by Trujillo et al. (2001a) as

$$C = 5 \log \left(\frac{r_{80}}{r_{20}} \right) \quad (1)$$

with r_f the radius containing a percentage f of the light of the galaxy, in this case 80 and 20 per cent, respectively. Other definitions using r_{90} and r_{50} are also in vogue, notably in the SDSS catalogue (see the discussion in Graham & Driver 2005). The radii are often taken from SExtractor (Bertin & Arnouts 1996; Holwerda 2005) output but we computed these here without the use of the SExtractor program. The two apertures for these radii are circular and hence this parameter is somewhat sensitive to the inclination of the spiral disc (see also Scarlata et al. 2007; Bendo et al. 2007, and Section 3.5). Concentration depends on the adopted central position for the measurement apertures.

3.1.2 Asymmetry

Following earlier work by Abraham et al. (1996b), the now most commonly used definition of Asymmetry is from Conselice (2003):

$$A = \frac{\Sigma_{i,j} |I(i,j) - I_{180}(i,j)|}{\Sigma_{i,j} |I(i,j)|} \quad (2)$$

where $I(i, j)$ is the value of the pixel at the position i, j in the image, and $I_{180}(i, j)$ is the value of the pixel in the same position in an image which is rotated 180° around the centre of the galaxy. To compute Asymmetry, we need a known position of the centre of the galaxy as well as a well-defined area. Abraham et al. (1996b) and Conselice (2003) apply a further correction to remove a contribution to the Asymmetry value by the sky background (see Section 3.4.1 for an explanation of why we did not choose to do so in this paper).

3.1.3 Smoothness

Following Takamiya (1999), Conselice (2003) introduced Smoothness, which has gone through several definitions. Here we use

$$S = \frac{\Sigma_{i,j} |I(i,j) - I_S(i,j)|}{\Sigma_{i,j} |I(i,j)|} \quad (3)$$

where $I_S(i, j)$ is the same pixel in a smoothed image. Smoothness is a parametrized version of the unsharp masking technique (Malin 1978) used on photographic plates to identify faint structures. The various definitions employ different smoothing kernels and sizes, the most recent one using a flexible kernel-size of 0.2 Petrosian

radius and the boxcar shape. To simplify matters, we chose to use a fixed 6 arcsec Gaussian smoothing for our definition. Abraham et al. (1996b) and Conselice (2003) apply a further correction for a background contribution to this parameter, which we did not do (see Section 3.4.1 for an explanation of why we did not do so).

3.2 Gini and M_{20}

The Gini and M_{20} parameters were established by Lotz et al. (2004) as an alternative to the CAS space.

3.2.1 Gini

The Gini parameter is an established qualifier in economics for the inequity in income for a population. For a Gini value of one, every person (or pixel) owns an equal fraction of the wealth (or flux). For a Gini value of zero, all wealth (or flux) is concentrated in a single person (or pixel). Abraham, van den Bergh & Nair (2003) introduced the Gini parameter, and Lotz et al. (2004) used this scale-invariant parameter to characterize the homogeneity of a galaxy image. This parameter shares some of the characteristics of Concentration and Smoothness from the CAS space but does not depend on the size and shape of a convolution kernel or the choice of the galaxy's centre. In Lotz et al. (2004), their equation (6), following the work by Glasser (1962), the Gini parameter can be redefined for speed if one orders the pixels according to value first:

$$G = \frac{1}{\bar{I}n(n-1)} \Sigma_i (2i - n - 1)|I_i| \quad (4)$$

where I_i is the value of pixel i in the ordered list, n is the number of pixels in the galaxy image and $\bar{I}$ is the mean pixel value in the image. We implemented this definition of the Gini parameter as the computationally least costly one.

3.2.2 M_{20}

Lotz et al. (2004) also introduce the relative second-order moment of the image to classify galaxies. The second-order moment of a pixel is: $M_i = I_i[(x_i - x_c)^2 + (y_i - y_c)^2]$, where I_i is the value of pixel i in the image, and x_i and y_i are the x and y coordinates of that pixel and x_c and y_c are the position of the galaxy's centre. The total second-order moment of an image is defined as

$$M_{\rm tot} = \Sigma M_i = \Sigma I_i[(x_i - x_c)^2 + (y_i - y_c)^2]. \quad (5)$$

When we now rank the pixels by value, we can define the relative second-order moment of the brightest 20 per cent of the flux:

$$M_{20} = \log\left(\frac{\Sigma_i^k M_i}{M_{\rm tot}}\right), \text{ for which } \Sigma_i^k I_i < 0.2 I_{\rm tot} \text{ is true.} \quad (6)$$

Pixel k is the pixel marking the 20 per cent point in the list of pixels ranked by flux value.

Some authors vary the central position (x_c, y_c) to minimize this parameter (Lotz et al. 2004; Bendo et al. 2007). Because we have dynamical centres, we fix x_c, y_c and treat deviations from this value as a source of uncertainty.

3.2.3 Ellipticity

Scarlata et al. (2007) added the ellipticity of a galaxy's image to the mix of parameters in order to classify galaxies according to type in the COSMOS field. Ellipticity is defined as

$$E = 1 - b/a \quad (7)$$

with a and b, the major and minor axes of the galaxy, computed from the spatial second-order moments of the light along the x and y axes of the image in the same manner as SExtractor (Bertin & Arnouts 1996; Holwerda 2005).

3.3 Uncertainty estimates

The sources of uncertainty in the above parameters are: (1) shot noise in the pixel values, (2) uncertainties in the position of the centre of the galaxy and (3) variations in the area over which the parameters are computed. The first two uncertainties can be estimated using a Monte Carlo set of iterations, and the last one using a jackknifing technique. The relative contribution of these sources of uncertainty depends on the instrument characteristics and hence wavelength, resolution and distance of the object. For instance, photon shot noise is more of an effect in UV and optical data, compared to the H I. Here, however, we treat each image the same and compute these uncertainties for the relevant parameters.

The shot noise effect on a parameter can be estimated by reassigning random pixel values around the mean value to each pixel in the image and recomputing the parameter several times. With a few iterations, the rms of the spread in parameter values is an estimate of uncertainty in the parameters.

Similarly, the uncertainty due to the measurement error of the centre of the galaxy (x_c, y_c) can be estimated by varying the input centre, recomputing the parameter and calculating the spread in values over a certain number of iterations (10 in our case). We use random deviations from x_c and y_c within a normal distribution with a width of 6 arcsec to mimic the uncertainty in the position of the centre.

The latter uncertainty estimate is important for Concentration, Asymmetry, M_{20} and Ellipticity as these depend on the assumed centre of the galaxy. To minimize our differences with dynamical parameters later, we adopted the dynamical centre from Trachternach et al. (2008) whenever possible. In previous optical high-redshift studies, the uncertainty in the position of the centre was considered less of an issue – since it is generally much less than a resolution element – but we find that for nearby galaxies, this is a substantial part of the error-budget in the parameters.

The Gini parameter does not depend on the central position and it is only weakly sensitive to shot noise in the pixel values. Therefore, we computed its uncertainty from a shot noise Monte Carlo set and the rms in Gini values from a series of subsets of the pixels in the image (a jackknife set). The jackknife approach to the Gini parameter uncertainty is advocated by Yitzhaki (1991). Gini shot noise and jackknife uncertainty estimates are of similar magnitude.

The reported uncertainties in Tables A3–A29 (in the electronic version of the article – see Supporting Information) are the combined uncertainty from shot noise and central position for all parameters, with the exception of the Gini parameter. In the case of Gini, the uncertainty is the combination of the shot noise estimate and the jackknife estimate. These are formal errors and in our opinion, the actual errors in these parameters are larger, predominantly due to viewing angle, resolution effects, image artefacts and remaining uncertainty about which pixels to include in the computation.

3.4 Systematics

There are several effects that may influence the structural parameters: (1) the sky background, notably any structure in this background, (2) the signal-to-noise ratio (S/N), (3) the inclination of

the disc and (4) the resolution and sampling of the instrument or conversely the distance of the galaxy. These systematics vary in prominence for each different wavelength but we focus on the effects on H I morphology here.

3.4.1 Background contribution

The sky and instrumental background in these images influence the morphological parameters in three different instances. First, the area over which the parameters are computed changes if an S/N criterion is used for the selection of pixels. Secondly, the *mean* sky background over the area contributes to the total parameter value. This is a de facto weighting of the shape contribution to the parameter. Thirdly, in the case of Asymmetry and Smoothness, the noise in the background adds value since these parameters use the absolute difference in pixel values.

The first consideration does not come into play in our experiment as we fixed the choice of area based on the H I contour. The contribution by the mean background is minimized in our case as we selected uniform data, which are already sky-subtracted, and we carefully sky-subtracted the SDSS tiles before addition. Especially the SINGS data were meticulously corrected for background contributions (see the fifth SINGS data release notes; SINGS Team 2006). The mean background contribution is dominated by the shape over which the parameters are computed. To compare, we include the parameters computed for the shape with all pixels set to unity in Appendix A (in the electronic version of the article – see Supporting Information, Figs A1–A27). This is effectively a gross overestimate of a *mean* background contribution. This leaves the noise term in Asymmetry and Smoothness as a separate problem.

Lotz et al. (2004) correct their Asymmetry and Smoothness values for a background contribution. Because these parameters use an absolute difference between pixels, any background noise – or other background contribution – will add to the signal in both these parameters. To correct for this, most authors estimate the background contribution in an area of similar size to the object, in either an aperture near or an annulus around the object. In the case of H I maps, this would be complicated by the fact that the H I map covers most of the field of view at the other wavelengths.

The reason we did not choose to correct our parameters for a background contribution this way was because the annulus where the background contribution would be computed for the inner contour would fall within the outer H I contour. Hence, the background may contain signal we are trying to measure. Using an annulus further out of the target galaxy is complicated by a lack of coverage in the optical and *Spitzer* images.

To test our assertion that the background contribution, which includes any flux by a background source that was not masked, is minimized, we compare the parameters in both contours in IRAC1 (3.6 μm) and MIPS 24 μm images, two filters for which we have measurements for all our galaxies. The 3.6 images were smoothed to 6 arcsec resolution, correlating the noise which would strengthen any weak background patterns, and the MIPS 24 was not smoothed but a likely candidate for background structure. Fig. 1 shows the comparison between the two contours. While there is much scatter, there is no systematic offset in either Asymmetry or Smoothness. Similar plots for the other wavelength show a similar trend. This represents a lower limit to a background structure contribution from, for example, instrument characteristics, etc. However, the lack of an offset is encouraging. The shot noise uncertainty (Section 3.3) is a separate effect from any background contribution but we note that, especially in Asymmetry, any background deviations seem to fall within the computed uncertainty.

Alternatively, one could construct background images, mimicking the background mean value and noise. However, if these do not include a mean background contribution, there is very little change in the values for all morphological parameters (at least for the 3.6 and 24 μm images where we tried this). The large S/N over many pixels in the selected shape dominates the parameter value.

Therefore, we do not correct our values for a background contribution here. However, these parameters have been determined for a large number of pixels and high S/N images of nearby galaxies. As soon as the background can be a substantial contribution to the intensities in an image, such is the case in *HST* images of distant galaxies, the background contribution needs to be revisited. In the case of H I observations in particular, this issue will be much less prominent as the column density map is constructed from high S/N line detections, lowering the relative contribution of the background.

3.4.2 Signal-to-noise ratio

Lotz et al. (2004) also conduct an experiment on how much these parameters are affected by a change in S/N. They find that G, M_{20} and C are reliable to within 10 per cent for galaxy images with S/N > 2 per pixel. Lisker (2008) find a similar S/N limit for the Gini parameter. Asymmetry and Smoothness decrease with S/N but stay within limits above S/N > 5. The stellar discs of all our galaxies are detected well beyond this noise level. The H I perspective will initially be used in the nearby Universe where the S/N level will comfortably exceed these limits because line detections exceed a S/N of 3 or 5 in individual channel maps to be included in the column density map. S/N effects will need to be considered when the classification scheme is applied to galaxies at higher redshifts with for instance SKA. The redistribution of pixel values around the mean (the Monte Carlo error estimate) in our parameter is in part to quantify how much effect noise has on our parameter determinations.

3.4.3 Distance effects on morphology

The accuracy of the morphological parameters depends on sampling and resolution of the analysed images. In addition, cosmological surface brightness dimming plays a role at greater distances. In this section, we focus on the effects of increasing distance on the morphological measurements in our H I column density maps, to ensure that these THINGS measures do not need to be corrected for relative distance.

Distance effects in the optical and infrared images have been discussed by both Lotz et al. (2004) and Bendo et al. (2007). Lotz et al. (2004) find that decreased sampling has the strongest effects on Concentration and M_{20}: 15 per cent changes when pixel scales become greater than 500 pc. Gini, Asymmetry and Smoothness, on the other hand, are relatively stable with decreasing spatial scales down to 1000 pc. In the near and far-infrared, Bendo et al. (2007) find that Concentration, Gini and near-infrared Asymmetry ($A_{3.6\,\mu\mathrm{m}}$) are invariant with image smoothing and the M_{20} parameter is only moderately affected (<20 per cent). The one exception is the Asymmetry in the far-infrared (24 μm). They report a dramatic change with distance; $A_{24\,\mu\mathrm{m}} \propto d^{-0.26}$, with d in Mpc. The spatial resolution of these 24 μm images is lower than the images at other wavelengths. However, they do sample smaller physical scales than

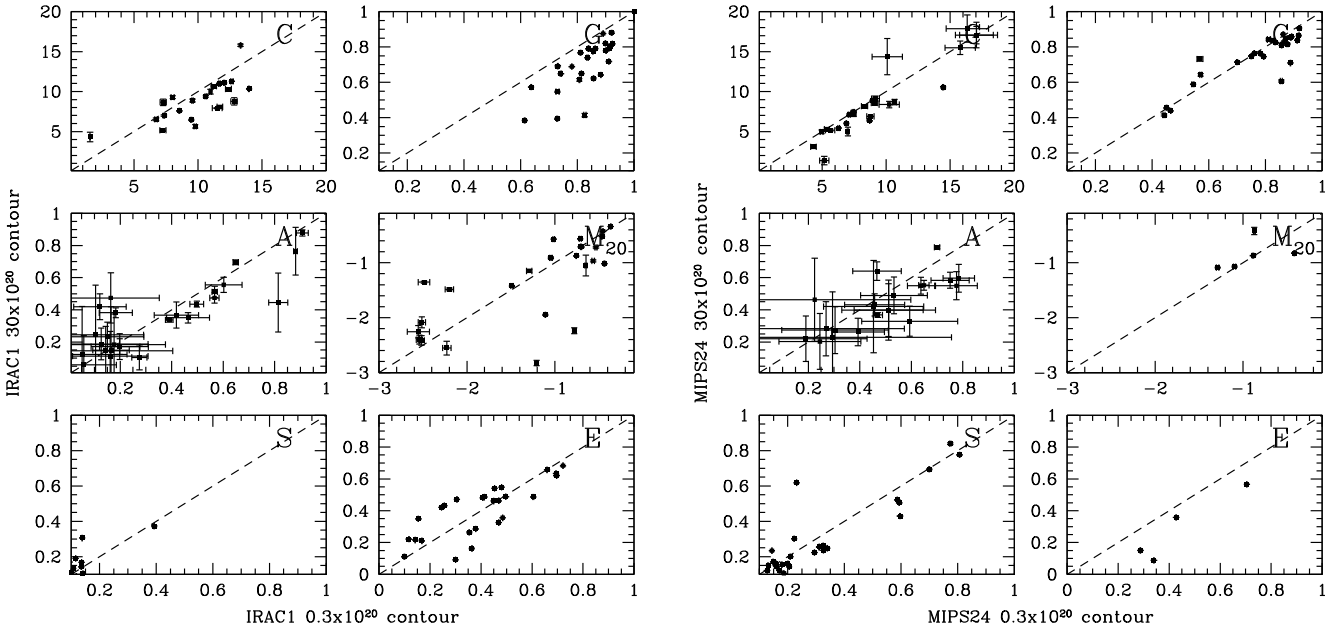

Figure 1. The morphological parameters for the smoothed IRAC1 (3.6 μm) and native resolution MIPS (24 μm) images for the gas disc contour and stellar disc contour. If there is a significant contribution by background noise to any of the parameters, this should manifest itself as an offset between the two contours.

the limit of 1 kpc found by Lotz et al. (2004) for the applicability of these parameters. The dramatic change in Asymmetry found by Bendo et al. seems to be somewhat in contradiction to the smooth decrease found by Lotz et al. The general picture is that as long as features smaller than 1 kpc are resolved in the images, the morphological parameters do not suffer too much but decline rapidly for coarser images.

The THINGS observations are designed to sample the H I at spatial scales below a kiloparsec but the future all-sky surveys will most likely sample the H I disc at lower spatial resolutions. To quantify the effects of distance on the morphological measurements, we use the H I RO maps of five face-on spiral galaxies: NGC 628, NGC 3184, NGC 3351, NGC 5457 and NGC 6946. To shift these to a series of distances, we cosmologically dimmed the maps, smoothed with 6 arcsec resolution at the appropriate distance, and resampled to the 1 arcsec pixel scale of the THINGS survey, adding the noise reported by Walter et al. (2008) for a single channel map (their table 2).[9]

In Fig. 2, we plot the ratio of the measured morphological parameter over the original, fiducial values (RO maps at the fiducial distance of zero).

Concentration and Smoothness of the H I maps are affected the most by distance effects. In the case of Smoothness, this is unsurprising as it relies on a smoothed version of the original image for the measurement. In the optical, the size of the smoothing kernel is adapted to be sensitive to specific scales of star formation. Hence, additional smoothing with distance is very likely to affect this value.

Asymmetry, Gini and M_{20} change less than 20 per cent in value with increasing distance. This is encouraging for their use throughout a local volume survey. Asymmetry certainly does not show the kind of behaviour described by Bendo et al. (2007) for the 24 μm SINGS maps (dotted line in Fig. 2). Considering the 24 μm images trace the dusty star formation and our maps trace the cool atomic gas, this is not as surprising as it initially appears. In the 24 μm maps, a large fraction of the flux is in a few star-forming regions, dominating morphological measurements. In the case of

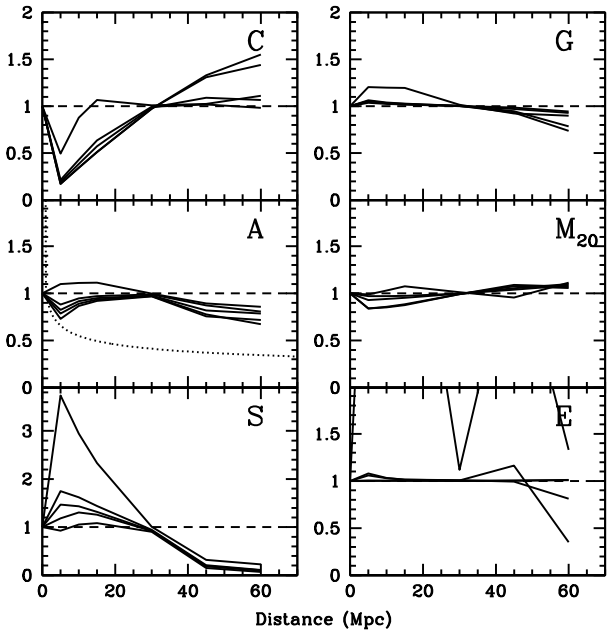

Figure 2. The effect of distance on H I galaxies. All morphological parameters are expressed as the ratio between the original value and the one found at greater distance. All five galaxies were dimmed, smoothed with the resolution of THINGS (6 arcsec) and regridded to the THINGS pixel scale (1 arcsec). The correction for Asymmetry with distance from Bendo et al. (2007) is marked with a dotted line (for *Spitzer*/MIPS data with 6 arcsec resolution).

[9] Our H I maps are observed throughout the data cube but we treat these maps as single images, similar to the redshifting prescription from Giavalisco et al. (1996).

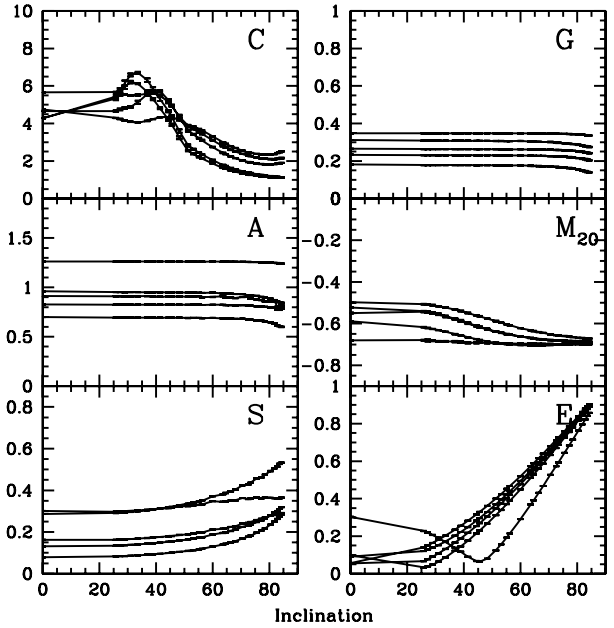

Figure 3. The changes in the values of the morphological parameters as a function of inclination of the disc. NGC 628, NGC 3184, NGC 3521, NGC 5457 and NGC 6946 were used. We assume that the H I discs are at zero inclination at the beginning and we rotate around the *Y*-axes.

H I, the morphology is determined by a large area with a very limited range of column densities. The difference in contrast for these observations may account for their different behaviour with increased distance. Ellipticity does not change in value much either. These galaxies have very low values of ellipticity as they are all near face-on.

In a companion paper in this series (Holwerda et al. 2011b), we quantify the effects of increased distance using simulated H I maps (initially at 150 pc sampling) and typical resolutions, pixel-scales and distances for current and planned surveys. From these simulated H I maps, it becomes clear that with current and planned observatories, morphological H I measurements are only useful for the very local volume.

3.5 Inclination effects

In the case of the Concentration defined by two circular apertures, the inclination dependence is an accepted feature, However, even in the case of elliptical apertures, there is often a remaining concentration–inclination relation. For example, Bendo et al. (2007) find that inclination influences the measured Concentration and they introduce a correction. Other parameters may well have subtle dependencies on the inclination of the disc. To explore these dependencies, we use the same five face-on galaxies as for the resolution simulations and rotate them around the *x*-axis assuming an infinitely thin disc for the H I emission (resampling solely along the *y*-axis). While these galaxies have some intrinsic inclination (see Table A1 in the electronic version of the article), we treat them as perfectly face-on as a starting point. Fig. 3 shows all six parameters as a function of inclination. A benefit of H I observations is a good new estimate of the inclination from the tilted ring fit to the velocity cube. Any correction for inclination will consequently be easy to perform for low-redshift galaxies.

Asymmetry, Smoothness and Gini are all relatively unaffected below an inclination of 80°, above which our assumption of a perfectly flat disc becomes tenuous. Ellipticity naturally changes drastically by inclining the disc. M_{20} converges to a value of -0.7. Concentration follows a complicated pattern peaking in the 30°–40° range. Bendo et al. (2007) find a much smoother correction of concentration for inclination, based on their elliptical apertures. Arguably, they pre-corrected for inclination by using an elliptical aperture whose shape depends on the inclination of the disc.

4 RESULTS

Appendix A (in the electronic version of the article – see Supporting Information) shows the column density maps and plots of the parameters over wavelength, and lists morphology parameter values for each of our 28 galaxies. The column density map of each galaxy shows the two areas in the images, corresponding to the extent of the gas (blue) and stellar (red) disc, defined by us as the 0.3 and 30 $\times$ 10^{20} cm^{-2} H I contours, respectively (or alternatively 0.24 and 24 M$_\odot$ pc^{-2}, respectively). We exclude those parts of the images where the H I map is below these values, even in the case of H I 'holes' in the H I disc. All six parameters, determined within these contours, are plotted for each wavelength we obtained data for. In order to compare different wavelengths, we defined the areas over which all the morphological parameters were computed exclusively based on the H I column density map. Appendix A also lists our brief notes on what we found for each galaxy in the literature, especially regarding its level of interaction. First we will compare our parameters to previous morphological results, and secondly to other measures of interaction.

4.1 Comparison to previous results

The SINGS sample, and hence the THINGS sample, has some overlap with the sample from Frei et al. (1996). Conselice (2003) presents CAS parameters for the Frei sample, and Lotz et al. (2004) present Gini, M_{20} and CAS parameters for the Frei sample, both in the optical *R*-band filter. Bendo et al. (2007) present Concentration, Asymmetry, Gini and M_{20} for two infrared wavelengths for the entire SINGS sample. Here, we compare our results for the H I contour corresponding to the stellar disc.

4.1.1 Optical

Conselice (2003) presents Concentration, Asymmetry and Smoothness in the *R* band for the Frei sample, and Lotz et al. (2004) present separate estimates of the CAS values as well as Gini and M_{20} for the Frei sample, in both *R* and *B* bands. The measurements from these two papers are the nearby (isolated) galaxy reference for CAS measurements. In Fig. 4 we compare the Conselice (2003) and Lotz et al. (2004) values, respectively, to ours for the *R*-band values for our 'stellar' disc (the 30 $\times$ 10^{20} cm^{-2} contour). The main difference between our implementation and the earlier work is the definition of the area over which the parameters are computed; we define the area over which the parameters are computed based on an H I contour. In contrast, both of the previously mentioned authors use an isophote in the optical or near-infrared image.[10] The Frei et al. images and

[10] Optical isophote and surface density contour are technically identical terms. We chose to use contour to emphasize that the choice of area is done based on the H I column density map, and not the optical images.

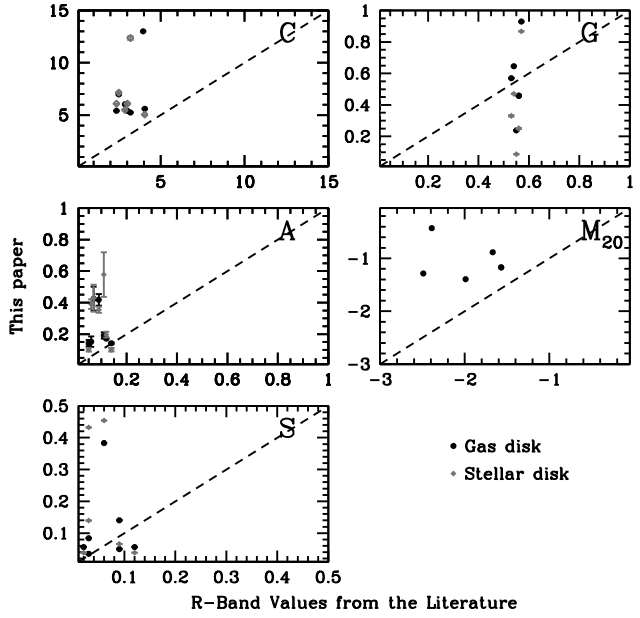

Figure 4. The *R*-band values for CAS from Conselice (2003) (left-hand panels) and Lotz et al. (2004) for the Gini and M_{20} parameters (right-hand panels).

the SINGS *R*-band ancillary data are not exactly the same in depth and filter which may result in additional differences.

There are some small differences in the parameter definitions as well. Both Conselice (2003) and Lotz et al. (2004) minimize the Asymmetry by allowing the galaxy's centre to vary. Bendo et al. (2007) and Lotz et al. (2004) have a similar approach to M_{20}. We chose to use the dynamical centre from Walter et al. (2008) and treated variations on it as an uncertainty.

The Gini values from Lotz et al. (2004) span a much smaller range than our values or those from Bendo et al. (2007), possibly because of the difference in area definition. Given that our areas are greater than those in Lotz et al., there is a relatively bigger contribution by a mass of low-intensity pixels, increasing the Gini parameter. Similarly, Bendo et al. compute the Gini value for a greater area (the RC3 ellipse), including many more low-flux pixels. This difference in area would explain higher values of Gini compared to Lotz et al., but not necessarily why there is a bigger spread in our values. In addition, Bendo et al. note that the active galactic nucleus (AGN) activity changes the IR values considerably and excludes the centre for some of their galaxies for this very reason. A central AGN is likely to be excluded automatically by an H I contour. Our concentration values for *R* band may well be higher if some central pixels are excluded by the H I contour (e.g. central H I hole in NGC 2841, Fig. A7). The difference in the M_{20} values is mostly due to the differences in area or possibly the depth of the data.

4.1.2 Infrared

Bendo et al. (2007) present values for Concentration, Asymmetry, Gini and M_{20} for the 3.6 and 24 μm images in the SINGS sample and by design our sample is a subset of this sample. Muñoz-Mateos et al. (2009) compare these infrared values to those in the UV. Both authors focus on their use for Hubble Type classifiers. Bendo et al. (2007) correct their Asymmetry values for distance and Concentration values for inclination. The other significant difference between our determination and that of Bendo et al. is that their result is from an elliptical aperture (defined by the de Vaucouleurs D_{25} in the RC3, de Vaucouleurs et al. 1991), and ours are for an H I contour.

Therefore, we recomputed our implementation of the morphological parameters (Concentration, Asymmetry and Gini and M_{20}) for the elliptical apertures used in Bendo et al. (2007). We placed the apertures centred on the galaxy position from Walter et al. (2008), using the minor and major axes from the NASA Extragalactic Data base (http://nedwww.ipac.caltech.edu/) and the Reference Catalog (RC3, de Vaucouleurs et al. 1991) position angle. Fig. 5 shows the values from Bendo et al. (2007) and ours. There is scatter in the values but that is to be expected as the input apertures, central positions and data are not perfectly identical. Concentration and Asymmetry are corrected by Bendo et al. for disc inclination and distance, respectively. We have uncorrected these values here for the comparison.

Our 3.6 μm Concentration and Gini values are higher than those from Bendo et al. This may be because Bendo et al. remove the contribution by the AGN in a few of their galaxies, as well as small differences in the adopted centre of the disc. There is substantial scatter in the M_{20} to higher values for 3.6 μm, and our Asymmetry values, for both 3.6 and 24 μm, are lower than the highest values for Asymmetry from Bendo et al. These differences are because we smooth the 3.6 μm data to 6 arcsec resolution. In addition, some of the differences in M_{20} and Asymmetry can be the result of slight differences in which pixels on the edge of the aperture are included in the computation. Both of these parameters weigh pixels in favour of those on the edge of the object.

All things considered, the values for these four parameters agree with the previous authors within our computed uncertainties. The smoothing effect should be kept in mind when comparing this paper's values to others but the smoothing is essential for the comparison across wavelength.

4.2 Morphology of star formation and H I

Because most of the existing work has been done at wavelengths dominated by recent star formation, mostly UV, we compare the morphological parameters determined in the H I RO maps to the parameters we determined in the NUV, FUV and MIPS 24 μm. The spatial resolutions in these wavelengths are all very similar, and we use the same two areas: the 3×10^{21} and 3×10^{19} cm^{-2} H I contours. Figs 6 , 7 and 8 show the six parameters computed in the far- and near-ultraviolet and 24 μm compared to the values in the RO H I maps.

Ellipticity translates extremely well from the UV to the H I. Concentration, M_{20} and Asymmetry also translate well but to a lesser extent. However, this can be expected for the H I disc. For instance, it was already known that gas discs are less concentrated, often with depressions in the centre of the galaxies. In the case of the Gini parameter, one could expect a shift because the range in values in an H I column density map is much smaller than the range in a UV flux map. Small changes in Asymmetry and M_{20} can be expected as a bright star-forming region does not necessarily translate into a high H I column density. Asymmetries for the H I and UV follow each other much better than the 24 μm emission. A similar relation is seen in M_{20} where H I and UV are reasonably similar but the 24 μm is not. Smoothness shows no clear relation.

In general, the morphological parameters from the far- or near-ultraviolet translate reasonably well to the H I, with the exceptions

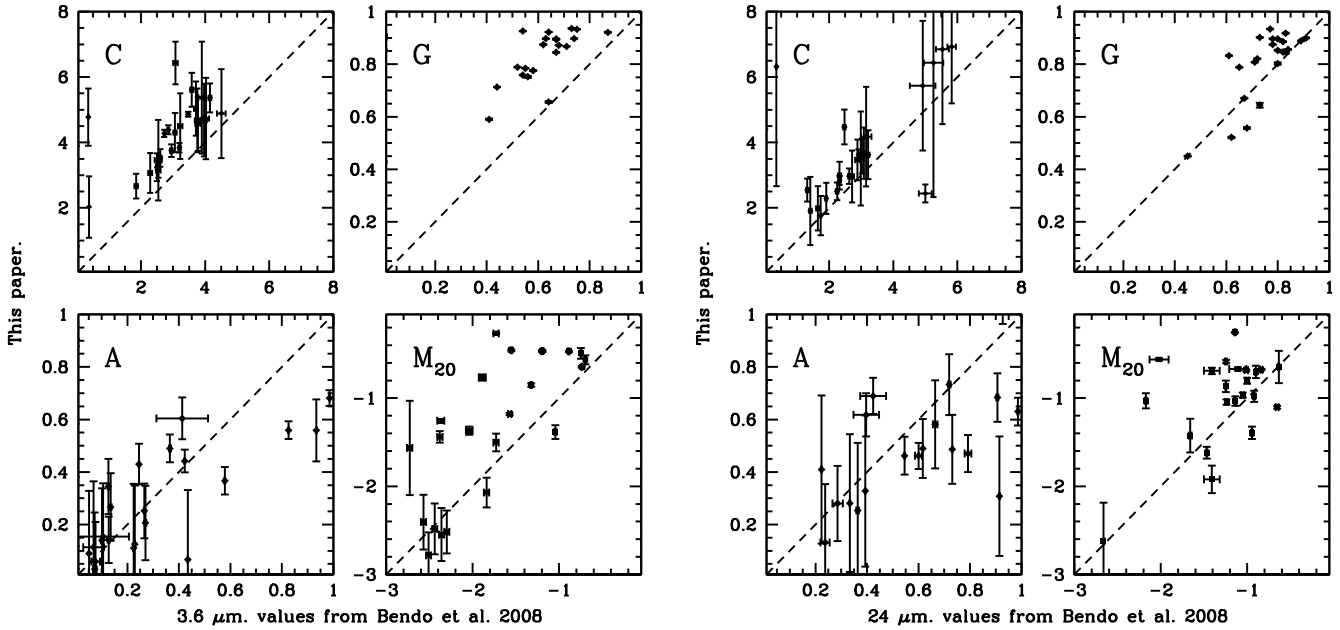

Figure 5. Our measurements of Concentration, Asymmetry, Gini and M_{20} in an elliptical aperture defined by the major and minor axes (D_{25}) from NED and the RC3 position angle for both the 3.6 and 24 μm images, compared to the values from Bendo et al. (2007). The dashed line is the line of equality.

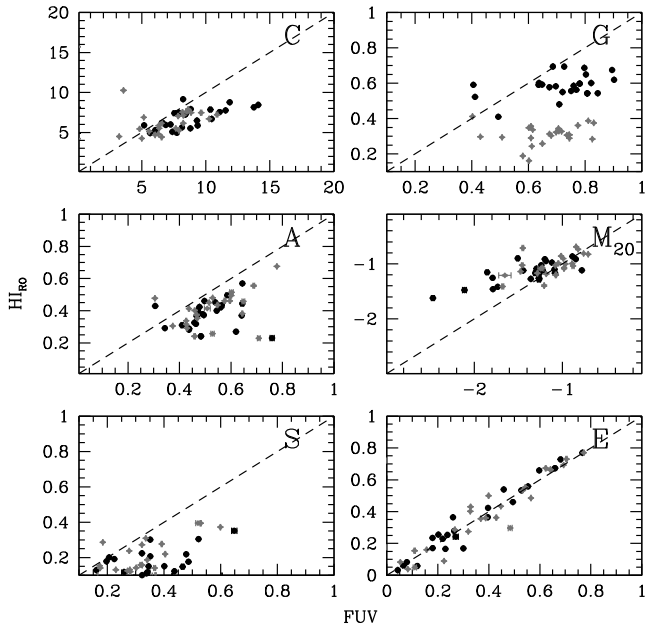

Figure 6. Our measurements of Concentration, Asymmetry, Smoothness, Gini, M_{20} and Ellipticity in both the stellar disc (3×10^{21} cm^{-2}, solid points) and the gas disc contour (3×10^{19} cm^{-2}, grey points) in far-ultraviolet compared to the values computed in the H I RO map.

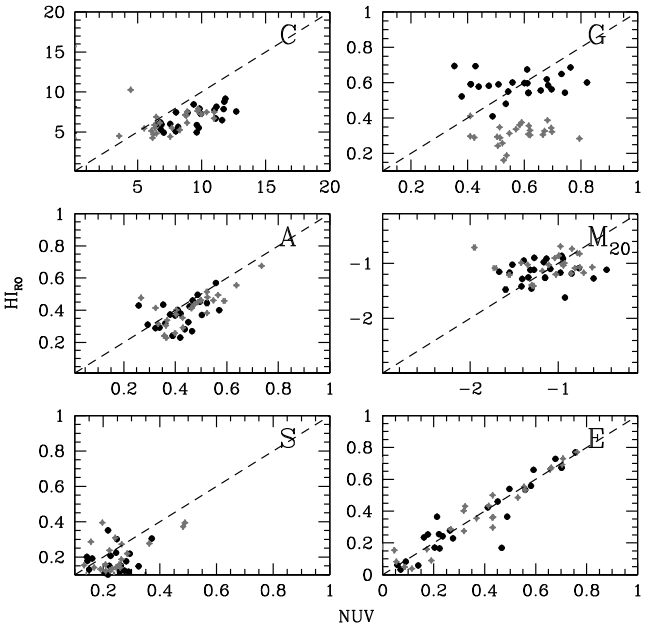

Figure 7. Our measurements of Concentration, Asymmetry, Smoothness, Gini, M_{20} and Ellipticity in both the stellar disc (3×10^{21} cm^{-2}, solid points) and the gas disc contour (3×10^{19} cm^{-2}, grey points) in near-ultraviolet compared to the values computed in the H I RO map.

(Concentration and Gini) well understood. The discrepancy is much greater with the 24 μm MIPS observations. Thus, H I and rest-frame ultraviolet merger measurements from morphology translate directly but any FIR morphology requires additional information. Arguably, FUV and H I trace the atomic ISM component and the 24 μm is more closely associated with the molecular (H_2) component. In favour of this argument is the poor relation in M_{20}; the bright pixels in 24 μm do not coincide with high column densities in H I. Fortunately, the majority of morphological measurements of mergers are in rest-frame UV and our measurements of merger fractions and rates should translate relatively directly.

5 SIGNATURES OF TIDAL INTERACTION

In this section, we explore the relation between other methods to determine the level of interaction for each galaxy and our morphological parameters. The level of interaction is difficult to quantify although some authors present a parametrization of the level of

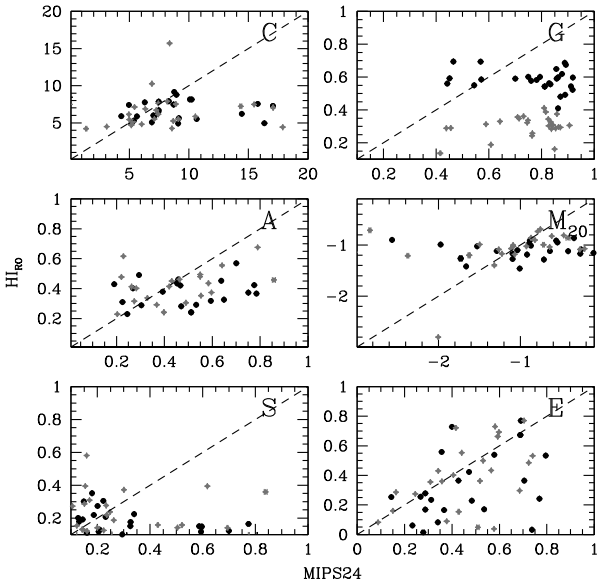

Figure 8. Our measurements of Concentration, Asymmetry, Smoothness, Gini, M_{20} and Ellipticity in both the stellar disc (3×10^{21} cm^{-2}, solid points) and the gas disc contour (3×10^{19} cm^{-2}, grey points) in *Spitzer* 24 μm compared to the values computed in the H I RO map.

tidal force on a galaxy (Karachentsev et al. 2004; Bournaud, Jog & Combes 2005). Alternatively, one can take the level of non-circular motion from the THINGS results as a measure of recent interaction. Many of these galaxies have been studied extensively and several previous authors have remarked upon signs of disturbance (see Table 1). In this section, we compare our morphological parameters in H I to these various parametrizations to identify those parameters that appear to be the most promising interaction tracers.

5.1 Tidal interaction parameter (Θ)

One way to measure the interaction rate is to find close galaxy pairs which, most likely, will be gravitationally interacting. Karachentsev et al. (2004) present a catalogue of neighbouring galaxies and a tidal estimate for each galaxy (Θ). Negative values of Θ correspond to isolated galaxies, and positive values are typical of group members. We should note that there are no completely isolated galaxies in our sample ($\Theta < 0$). Only NGC 628 and NGC 2403 have $\Theta = 0$; galaxies in average density environments. We note that NGC 2403 was the zero-point calibrator for this tidal parameter. Five galaxies have no value for Θ (NGC 2841, NGC 3198, NGC 3521, NGC 5055, NGC 7331). This makes a direct comparison between the morphological parameters and tidal interaction more difficult. Fig. 9 shows no clear relation between any of the morphological parameters of the H I maps and Θ, compared over either the optical or the gas disc.

Because we only have one galaxy with a high value of the Karachentsev tidal estimate ($\Theta = 4$ for NGC 5194), we can only glean trends with this parameter: compared to the locus of group galaxies, the M_{20} parameter for the H I map appears to be higher for NGC 5194, and Concentration, Asymmetry and Gini show a slight trend. We interpret the relation with Θ as useful to point out those parameters that could be of use to identify mergers in

Table 1. The ranking of interaction.

	Name	Notes	Reference
1.	NGC 2841	H I warp	
2.	NGC 3184		
3.	NGC 3521		
4.	NGC 3621		
5.	NGC 3198	Strong non-circular motion	Trachternach et al. (2008)
6.	NGC 2903	Small companion	Irwin et al. (2009)
7.	NGC 628	High-velocity clouds	Kamphuis & Briggs (1992)
8.	NGC 925	H I tail	Sancisi et al. (2008)
9.	NGC 5457	Lopsided	Richter & Sancisi (1994)
10.	NGC 6946	Holes, high-velocity complexes	Boomsma et al. (2008)
11.	NGC4736	H I streaming in and lopsided.	
12.	NGC 7793	Sculptor Group member, warp	
13.	NGC 7331	Proximity to Stephanïs Quintet	Gutiérrez et al. (2002)
14.	NGC 2403	M81 group member, extra-planar H I	Fraternali et al. (2002)
15.	Holmberg II	M81 group member	Stewart et al. (2000)
16.	M81A	M81 group member	
17.	DDO 53	M81 group member	
18.	Holmberg I	M81 group member	
19.	NGC 2976	M81 group member	
20.	IC 2574	M81 group member, H I supershell	
21.	NGC 3031	M81 central galaxy	
22.	NGC 3627	Member interacting Leo triplet	
23.	NGC 5194	Canonical 3:1 interaction	
24.	NGC 5055	Extended spiral structures, H I warp	Bosma (1981)
25.	NGC 4826	Counter-rotating H I disc	Braun et al. (1994)
26.	NGC 5236	High-velocity clouds, stellar and H I streams and an H I warp.	Malin & Hadley (1997) Radburn-Smith et al. (2011)

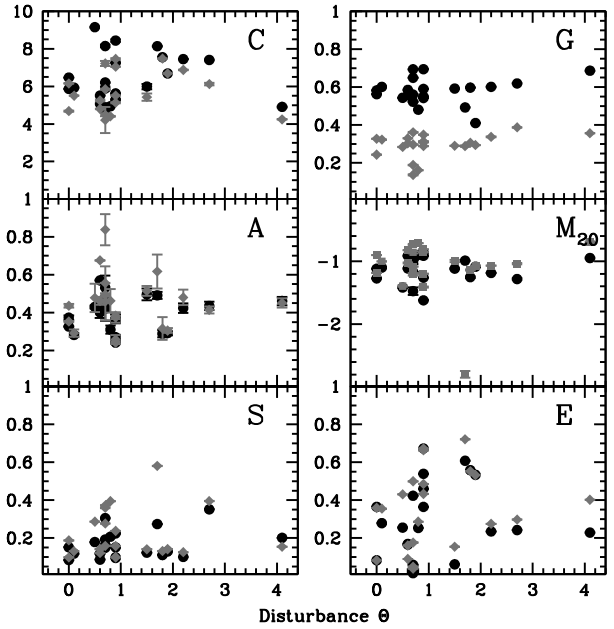

Figure 9. All six morphological parameters, Concentration, Asymmetry, Smoothness, Gini, M_{20} and Ellipticity as a function of tidal disturbance (Θ) from Karachentsev et al. (2004). Grey points are for the outer contour (the gas disc) and the solid points for the inner contour (the stellar disc).

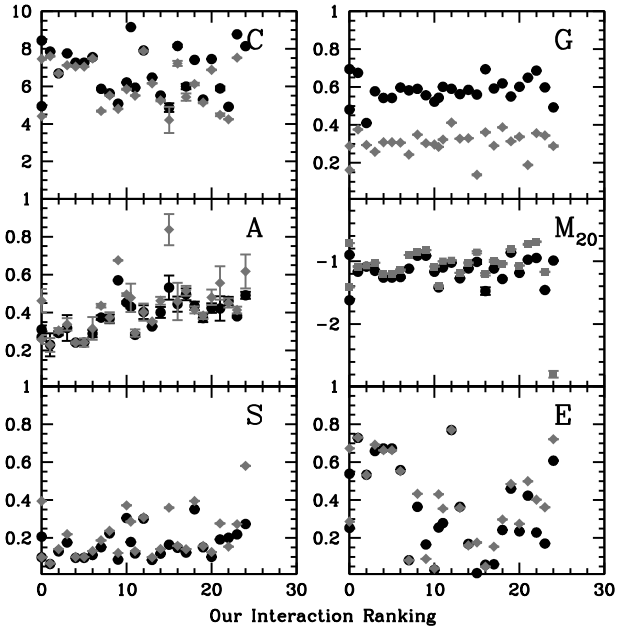

Figure 10. All six morphological parameters, Concentration, Asymmetry, Smoothness, Gini, M_{20} and Ellipticity as a function of our ranking. Grey points are computed over the gas disc and solid points for the inner stellar contour. We note the marked increase in Asymmetry.

H I morphology, but the THINGS sample does not have the spread in Θ to isolate the H I morphological parameter space where gravitational interactions reside.

5.2 Interaction ranking

Because the THINGS sample was mostly chosen to include nearby and non-interacting galaxies (M51 being the obvious exception), the majority of the above galaxies are not in the stage of an interaction where the morphological signature is the strongest (Lotz et al. 2008b, 2010a,b). So much so that Smith et al. (2007) use the SINGS sample (minus M51) as their reference for non-interacting galaxies. However, we can rank the THINGS galaxies on the level of interaction signature reported in the literature. In Table 1 we rank the sample based on the plausible stage of interaction from isolated, non-harassed galaxies to merger and merger remnant. This ranking is subjective as more information on a galaxy (such as high-resolution H I data) often reveals signs of mild interaction (e.g. warps or low column density structures), and it is still unclear what signatures are from interaction or not. For instance, warps may be formed by other means as well (e.g. IGM ram pressure). Certain features are long lived (e.g. warps) while others fade relatively quickly (tidal arms). Fig. 10 shows all six parameters as a function of the ranking in Table 1. Asymmetry shows a gradient with the ranking while M_{20} does not. In our opinion, this does not mean that Asymmetry is a better parameter to detect interaction; it is very sensitive and may well pick up other effects or longer lasting effects as well.

5.3 Non-circular motions

Trachternach et al. (2008) report a measure of the relative non-circular motion in a subset of the THINGS galaxies; the total power in the non-circular harmonic components over the maximum velocity in the rotation curve ($A_r/v_{\rm max}$). They report amplitudes of the non-circular motions lower than expected for the steep central mass

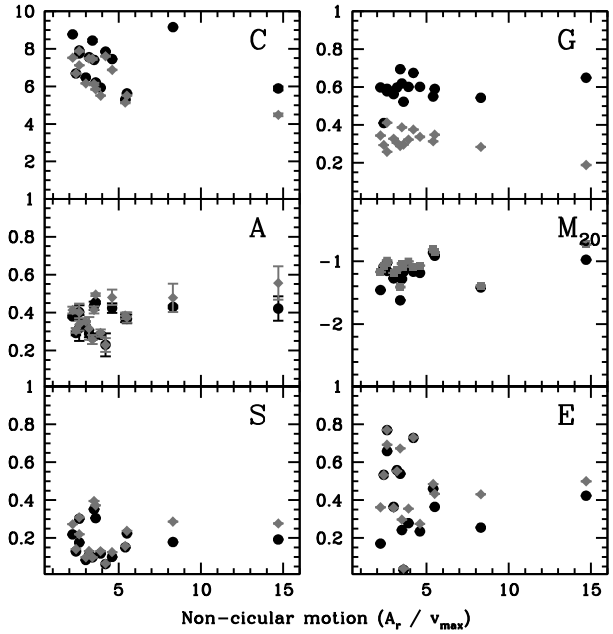

Figure 11. All six morphological parameters, Concentration, Asymmetry, Smoothness, Gini, M_{20} and Ellipticity as a function of the non-circularity of the H I kinematics in the disc according to Trachternach et al. (2008). Grey points are the gas disc, and solid points are computed for the inner stellar contour.

density predicted by ΛCDM numerical simulations. This THINGS subset of 19 galaxies was selected to be non-interacting, limiting our comparison here. In Fig. 11, we plot the morphological parameters as a function of relative non-circular strength. At best, there seem to be only very weak trends between Concentration, Asymmetry and M_{20} with the relative non-circular motion (A_r). However, the highest value of A_r (NGC 3627) is a close group member

(there is no A_r value for M51). Thus, morphological and dynamical parameters combined may delineate a superb space to identify mergers and harassed galaxies. Future large surveys will have both dynamical information (e.g. measured by GALAPAGOS) and morphological information from these parameters, opening the possibility for a combined identification of disturbed galaxies.

6 DISCUSSION

In this paper we present our determinations of six morphological parameters computed within an inner and outer contour, approximately corresponding to the stellar and gas disc of these spirals. We aimed to determine how well H I morphology can serve as an indicator of tidal interaction. There is much anecdotal evidence for this but the parametrization used to date mostly in rest-frame ultraviolet images offers a way to quantify. We selected the THINGS sample as it is nearby, mostly comprising spirals, and offers many excellent ancillary data. We tried to answer the following questions: which disc size (stellar or gas) works best to determine the H I morphology? How well does the H I morphology compare to others used for interaction so far? Which parameters are the best indicators of interaction in H I?

6.1 Which wavelength shows interaction?

From the morphology–wavelength plots in Appendix A (in the electronic version of the article – see Supporting Information), as well as Figs 6, 7 and 8, it is apparent that the wavelength at which the parameter is determined is very important. Ultraviolet and the H I parameters appear to correlate as these trace star formation and some of its fuel or alternatively massive stars and the atomic component due to their photodissociation (Allen, Heaton & Kaufman 2004). Future H I results on interaction rates of spirals should be very similar to ultraviolet determined ones.

Indeed, the sensitivity of H I observations to gas-rich and minor mergers is a critical benefit as these types dominate the mergers at higher redshift (Lotz et al. 2010a, b). The all-sky surveys envisaged will then provide a valuable local reference for the characterization of these types of mergers. The added benefits are that H I appears to be very sensitive to gravitational interaction and there is no lag time waiting for star formation to occur. On the other hand, H I morphology may be uniquely sensitive to other phenomena, such as ram-pressure stripping.

6.2 Which disc size works best?

The wavelength at which these parameters are determined is critical [see the figures in Appendix A of individual galaxies (in the electronic version of the article – see Supporting Information) or Figs 6–8], but which choice of area is optimal to compute these parameters? There is some extra information in optical morphological parameters if they are computed over the extent of the gas disc (3×10^{19} cm^{-2} contour) as opposed to the stellar disc (3×10^{21} cm^{-2} contour). Notably, ultraviolet, *Spitzer* 24 μm, and especially of course the H I change with increased area. In the case of UV, this is partly because the sky level and noise are so low that a signal is easier to pick out. The compatibility is good news if we want to compare future H I results, computed for the whole gas disc, to those found by other authors on rest-frame ultraviolet discs.

6.3 Which parameters are indicators of interaction?

The main limitation to answering this question is the choice of sample as the THINGS sample was originally chosen as a relatively quiescent reference sample; most THINGS galaxies are group members. With the exception of M51, there are no ongoing mergers. In previous studies, both the Asymmetry and M_{20} parameters were used to identify strongly perturbed systems in *HST* deep fields. The H I value of these does seem to follow those in the FUV and NUV relatively closely, which is promising but not conclusive. If one compares the tidal parameter or our ranking for the bulk of the THINGS sample, there is a gentle rise in Asymmetry that one would not expect if this parameter is exclusively dependent on interaction, yet the M_{20} parameter for M51's stellar disc does not seem out of place with the rest of the THINGS and VIVA[11] sample. Interestingly, the M_{20} value for the entire gas disc does seem to deviate somewhat (Fig. 9). Therefore, we speculate here that a combination of these two parameters may yield the best result in identifying merging or strongly interacting systems. In our following papers, Holwerda et al. (2011a,b), this speculation is borne out by a large sample of H I maps and simulations of the H I column density maps during a merger.

7 CONCLUSIONS

From our multi-wavelength analysis of the quantified morphology of 28 galaxies in the THINGS survey, we conclude the following.

(1) The H I morphology in column density maps down to approximately 10^{20} cm^{-2} is a promising perspective on galaxy interactions. Many of the H I parameters show a close link to those in the near- and far-ultraviolet, which have been used to date to morphologically identify ongoing mergers. Concentration, Asymmetry and Ellipticity appear to be closely linked; Smoothness and M_{20} show a noisier relation between H I and UV morphological parameters and the Gini parameter is the notable exception with little correlation between the H I and UV determined values.

(2) Despite the close link between far- and near-ultraviolet and H I morphology, the wavelength at which the morphological parameter is measured is key, with the choice of area over which the parameters are computed being of secondary importance. This has some implications for comparing morphological parameters across different studies, especially if these were done at different wavelengths. The only exception seems to be the UV and H I morphologies, which can be compared more directly. An increase in sensitivity of the H I maps, or a corresponding decrease in H I contour level, only affects the Gini parameter due to the addition of many more low-value data points. The remaining morphological parameters are not affected. This is encouraging for studies comparing H I morphologies in maps with different depths.

(3) There are, at best, only weak trends between Concentration, Asymmetry and M_{20} and the non-circular motion strength ($A_r/v_{\rm max}$) (Fig. 11). This may imply that H I morphological and kinematic deviations can be complementary tracers of disturbances of the spiral disc.

(4) The two most common morphological parameters to identify mergers, Asymmetry and M_{20}, show contradictory behaviour in H I. Asymmetry seems to be very sensitive to disturbances, such as interaction, but also other phenomena (starburst, etc.), while M_{20} may be somewhat too insensitive (Figs 9 and 10). Based on

[11] VLA Imaging of Virgo spirals in Atomic gas (Chung et al. 2009).

the THINGS sample, which admittedly does not span a sufficient range of gravitational interaction, we speculate that a combination of these two parameters may be useful for merger selection based on H I morphology.

In the future, the high-resolution H I maps of THINGS can serve as an excellent reference because these spirals are in just the type of small groups that the majority of spirals reside in. Bigger H I surveys such as the WHISP project (van der Hulst et al. 2001; van der Hulst 2002), and those to be undertaken with APERTIF, ASKAP, EVLA, MeerKAT and eventually SKA will provide ever increasing statistics on the H I morphology of spirals. Using some of these bigger samples, we hope to identify the part of H I morphology space which corresponds to ongoing mergers. In the following papers in this series, we aim to quantify morphology to the WHISP sample on H I column density maps, identify the merger space for H I morphology, the time-scale over which mergers are visible, and ultimately infer a merger rate based on the WHISP sample.

ACKNOWLEDGMENTS

We thank the THINGS, SINGS, SDSS and *GALEX* collaborations for making their data public. The authors would like to thank the anonymous referee for his or her careful work which led to a substantial improvement of this paper. The authors would like to thank W. Clarkson and J. Lotz for comments and discussions. We acknowledge support from the National Research Foundation of South Africa. The work of BWH and WJGdB is based upon research supported by the South African Research Chairs Initiative of the Department of Science and Technology and the National Research Foundation. AB acknowledges the financial support from the South African Square Kilometer Array Project. Research based on public data from *GALEX*, SDSS, *Spitzer* and the VLA. The National Radio Astronomy Observatory is a facility of the National Science Foundation operated under cooperative agreement by Associated Universities, Inc. This work is based in part on observations made with the *Spitzer Space Telescope*, which is operated by the Jet Propulsion Laboratory, California Institute of Technology under a contract with NASA. Funding for the SDSS and SDSS-II has been provided by the Alfred P. Sloan Foundation, the Participating Institutions, the National Science Foundation, the US Department of Energy, the National Aeronautics and Space Administration, the Japanese Monbukagakusho, the Max Planck Society and the Higher Education Funding Council for England. The SDSS Web Site is http://www.sdss.org/. The SDSS is managed by the Astrophysical Research Consortium for the Participating Institutions. The Participating Institutions are the American Museum of Natural History, Astrophysical Institute Potsdam, University of Basel, University of Cambridge, Case Western Reserve University, University of Chicago, Drexel University, Fermilab, the Institute for Advanced Study, the Japan Participation Group, Johns Hopkins University, the Joint Institute for Nuclear Astrophysics, the Kavli Institute for Particle Astrophysics and Cosmology, the Korean Scientist Group, the Chinese Academy of Sciences (LAMOST), Los Alamos National Laboratory, the Max-Planck-Institute for Astronomy (MPIA), the Max-Planck-Institute for Astrophysics (MPA), New Mexico State University, Ohio State University, University of Pittsburgh, University of Portsmouth, Princeton University, the United States Naval Observatory and the University of Washington. This work is based on observations made with the NASA *Galaxy Evolution Explorer*. *GALEX* is operated for NASA by the California Institute of Technology under NASA contract NAS5-98034. This research has made use of the NASA/IPAC Extragalactic Data base (NED) which is operated by the Jet Propulsion Laboratory, California Institute of Technology, under contract with the National Aeronautics and Space Administration. In memory of Dr M. J. Holwerda.

REFERENCES

Abraham R. G., Valdes F., Yee H. K. C., van den Bergh S., 1994, ApJ, 432, 75
Abraham R. G., Tanvir N. R., Santiago B. X., Ellis R. S., Glazebrook K., van den Bergh S., 1996a, MNRAS, 279, L47
Abraham R. G., van den Bergh S., Glazebrook K., Ellis R. S., Santiago B. X., Surma P., Griffiths R. E., 1996b, ApJS, 107, 1
Abraham R. G., van den Bergh S., Nair P., 2003, ApJ, 588, 218
Allen R. J., Heaton H. I., Kaufman M. J., 2004, ApJ, 608, 314
Bendo G. J. et al., 2007, MNRAS, 380, 1313
Bershady M. A., Jangren A., Conselice C. J., 2000, AJ, 119, 2645
Bertin E., Arnouts S., 1996, A&AS, 117, 393
Boomsma R., Oosterloo T. A., Fraternali F., van der Hulst J. M., Sancisi R., 2008, A&A, 490, 555
Booth R. S., de Blok W. J. G., Jonas J. L., Fanaroff B., 2009, preprint (arXiv:0910.2935)
Bosma A., 1981, AJ, 86, 1825
Bournaud F., Jog C. J., Combes F., 2005, A&A, 437, 69
Braun R., Walterbos R. A. M., Kennicutt R. C., Jr, Tacconi L. J., 1994, ApJ, 420, 558
Bundy K., Ellis R. S., Conselice C. J., 2005, ApJ, 625, 621
Carilli C. L., Rawlings S., 2004, New Astron. Rev., 48, 979
Chung A., van Gorkom J. H., Kenney J. D. P., Crowl H., Vollmer B., 2009, AJ, 138, 1741 (Erratum: 2010, AJ, 139, 2716)
Conselice C. J., 2003, ApJS, 147, 1
Conselice C. J., Bershady M. A., Jangren A., 2000, ApJ, 529, 886
Conselice C. J., Yang C., Bluck A. F. L., 2009, MNRAS, 361
Darling J., Giovanelli R., 2006, AJ, 132, 2596
de Blok W. J. G., Walter F., Brinks E., Trachternach C., Oh S.-H., Kennicutt R. C., 2008, AJ, 136, 2648
de Blok W. J. G., Jonas J., Fanaroff B., Holwerda B. W., Bouchard A., Blyth S., van der Heyden K., Pirzkal N., 2009, in Serra P., Heald G., eds, Panoramic Radio Astronomy: Wide field 1–2 GHz Research on Galaxy Evolution. SISSA, http://pos.sissa.it
de Ravel L. et al., 2009, A&A, 498, 379
de Vaucouleurs G., de Vaucouleurs A., Corwin H. G., Buta R. J., Paturel G., Fouque P., 1991, Third Reference Catalogue of Bright Galaxies, Vol. 1–3. Springer-Verlag, Berlin, p. 2069
Fraternali F., van Moorsel G., Sancisi R., Oosterloo T., 2002, AJ, 123, 3124
Frei Z., Guhathakurta P., Gunn J. E., Tyson J. A., 1996, AJ, 111, 174
Giavalisco M., Livio M., Bohlin R. C., Macchetto F. D., Stecher T. P., 1996, AJ, 112, 369
Glasser G. J., 1962, J. Am. Stat. Assoc., 57, 648
Graham A. W., Driver S. P., 2005, Publ. Astron. Soc. Australia, 22, 118
Gutiérrez C. M., López-Corredoira M., Prada F., Eliche M. C., 2002, ApJ, 579, 592
Hibbard J. E., van Gorkom J. H., Rupen M. P., Schiminovich D., 2001, in Hibbard J. E., Rupen M., van Gorkom J. H., eds, ASP Conf. Ser. Vol. 240, Gas and Galaxy Evolution. Astron. Soc. Pac., San Francisco, p. 657
Holwerda B. W., 2005, preprint (astro-ph/0512139)
Holwerda B. W., de Blok W. J. G., Bouchard A., Blyth S., van der Heyden K., Pirzkal N., 2009, preprint (arXiv:0908.0693)
Holwerda B. W., Pirzkal N., de Blok W. J. G., Bouchard A., Blyth S.-L., van der Heyden K. J., Elson E. C., 2011a, MNRAS, in press (doi:10.1111/j.1365-2966.2011.17683.x)
Holwerda B. W., Pirzkal N., Cox T. J., de Blok W. J. G., Weniger J., Bouchard A., Blyth S.-L., van der Heyden K. J., 2011b, MNRAS, in press (doi:10.1111/j.1365-2966.2011.18940.x)

Holwerda B. W., Pirzkal N., de Blok W. J. G., Bouchard A., Blyth S.-L., van der Heyden K. J., 2011c, MNRAS, in press (doi:10.1111/j.1365-2966.2011.18942.x)
Holwerda B. W., Pirzkal N., de Blok W. J. G., van Driel W., 2011d, MNRAS, in press (doi:10.1111/j.1365-2966.2011.18662.x)
Hopkins P. F. et al., 2010, ApJ, 724, 915
Irwin J. A. et al., 2009, ApJ, 692, 1447
Jogee S. et al., 2009, ApJ, 697, 1971
Johnston S. et al., 2008, Exp. Astron., 22, 151
Jonas J., 2007, in Beswick R., ed., From Planets to Dark Energy: the Modern Radio Universe. SISSA, http://pos.sissa.it, p. 7
Kamphuis J., Briggs F., 1992, A&A, 253, 335
Karachentsev I. D., Karachentseva V. E., Huchtmeier W. K., Makarov D. I., 2004, AJ, 127, 2031
Kennicutt R. C. et al., 2003, PASP, 115, 928
Klöckner H., Baan W. A., 2005, Ap&SS, 295, 277
Lee J. C. et al., 2008, in Funes J. G., Corsini E. M., eds, ASP Conf. Ser. Vol. 396, Formation and Evolution of Galaxy Disks. Astron. Soc. Pac., San Francisco, p. 151
Lisker T., 2008, ApJS, 179, 319
Lotz J. M., Primack J., Madau P., 2004, AJ, 128, 163
Lotz J. M. et al., 2008a, ApJ, 672, 177
Lotz J. M., Jonsson P., Cox T. J., Primack J. R., 2008b, MNRAS, 391, 1137
Lotz J. M., Jonsson P., Cox T. J., Primack J. R., 2010a, MNRAS, 404, 590
Lotz J. M., Jonsson P., Cox T. J., Primack J. R., 2010b, MNRAS, 404, 575
Malin D. F., 1978, Nat, 276, 591
Malin D., Hadley B., 1997, in Arnaboldi M., Da Costa G. S., Saha P., eds, ASP Conf. Ser. Vol. 116, The Nature of Elliptical Galaxies: 2nd Stromlo Symposium. Astron. Soc. Pac., San Francisco, p. 460
Muñoz-Mateos J. C. et al., 2009, ApJ, 703, 1569
Murphy T. W., Jr, Soifer B. T., Matthews K., Armus L., 2001, ApJ, 559, 201
Napier P. J., 2006, in Backer D. C., Moran J. M., Turner J. L., eds, ASP Conf. Ser. Vol. 356, Revealing the Molecular Universe: One Antenna is Never Enough. Astron. Soc. Pac., San Francisco, p. 65
Patton D. R., Carlberg R. G., Marzke R. O., Pritchet C. J., da Costa L. N., Pellegrini P. S., 2000, ApJ, 536, 153
Radburn-Smith D. J. et al., 2011, ApJS, 195, 18
Ravindranath S. et al., 2006, ApJ, 652, 963
Richter O.-G., Sancisi R., 1994, A&A, 290, L9
Sancisi R., Fraternali F., Oosterloo T., van der Hulst T., 2008, A&AR, 15, 189
Scarlata C. et al., 2007, ApJS, 172, 406
SINGS Team, 2006, SINGS Fifth Data Delivery Release Notes
Smith B. J., Struck C., Hancock M., Appleton P. N., Charmandaris V., Reach W. T., 2007, AJ, 133, 791
Springel V. et al., 2005, Nat, 435, 629
Stewart S. G. et al., 2000, ApJ, 529, 201
Takamiya M., 1999, ApJS, 122, 109
Taylor-Mager V. A., Conselice C. J., Windhorst R. A., Jansen R. A., 2007, ApJ, 659, 162
Trachternach C., de Blok W. J. G., Walter F., Brinks E., Kennicutt R. C., 2008, AJ, 136, 2720
Trujillo I., Aguerri J. A. L., Cepa J., Gutiérrez C. M., 2001a, MNRAS, 328, 977
Trujillo I., Aguerri J. A. L., Gutiérrez C. M., Cepa J., 2001b, AJ, 122, 38
Trujillo I., Graham A. W., Caon N., 2001c, MNRAS, 326, 869
Trujillo I., Conselice C. J., Bundy K., Cooper M. C., Eisenhardt P., Ellis R. S., 2007, MNRAS, 382, 109
van der Hulst J. M., 2002, in Taylor A. R., Landecker T. L., Willis A. G., eds, ASP Conf. Ser. Vol. 276, Seeing Through the Dust: The Detection of H I and the Exploration of the ISM in Galaxies. Astron. Soc. Pac., San Francisco, p. 84
van der Hulst J. M., van Albada T. S., Sancisi R., 2001, in Hibbard J. E., Rupen M., van Gorkom J. H., eds, ASP Conf. Ser. Vol. 240, Gas and Galaxy Evolution. Astron. Soc. Pac., San Francisco, p. 451
Verheijen M. A. W., Oosterloo T. A., van Cappellen W. A., Bakker L., Ivashina M. V., van der Hulst J. M., 2008, in Minchin R., Momjian E., eds, AIP Conf. Ser. Vol. 1035, The Evolution of Galaxies Through the Neutral Hydrogen Window. Am. Inst. Phys., New York, p. 265
Walter F., Brinks E., de Blok W. J. G., Bigiel F., Kennicutt R. C., Thornley M. D., Leroy A., 2008, AJ, 136, 2563
Yan H. et al., 2005, ApJ, 634, 109
Yitzhaki S., 1991, Am. Stat. Assoc., 9, 235

SUPPORTING INFORMATION

Additional Supporting Information may be found in the online version of this article:

Appendix A. Morphological parameters, input and notes.

Please note: Wiley-Blackwell are not responsible for the content or functionality of any supporting materials supplied by the authors. Any queries (other than missing material) should be directed to the corresponding author for the article.

This paper has been typeset from a TEX/LATEX file prepared by the author.